Journal of Alloys and Compounds 845 (2020) 156355

Contents lists available at ScienceDirect

Journal of Alloys and Compounds

journal homepage: http://www.elsevier.com/locate/jalcom

Magnetization spin reversal and neutron diffraction study of polycrystalline $Tb_{0.55}Sr_{0.45}MnO_3$

Harshit Agarwal [a, **], Jose.A. Alonso [b], Ángel Muñoz [c], R.J. Choudhary [d], O.N. Srivastava [a], M.A. Shaz [a, *]

[a] Department of Physics, Institute of Science, Banaras Hindu University, Varanasi, 05, India
[b] Instituto de Ciencia de Materiales de Madrid, CSIC, Cantoblanco, E-28049, Madrid, Spain
[c] Departamento de Física Aplicada, EPS, Universidad Carlos III, Avenida Universidad 30, E-28911, Leganés, Madrid, Spain
[d] UGC-DAE Consortium of Scientific Research, Indore, India

ARTICLE INFO

Article history:
Received 4 June 2020
Received in revised form
7 July 2020
Accepted 8 July 2020
Available online 11 July 2020

Keywords:
Manganite
Neutron diffraction
Spin reversal
Magnetic study

ABSTRACT

We have investigated the structural and magnetic phase transitions in Sr doped polycrystalline $Tb_{0.55}Sr_{0.45}MnO_3$, using temperature-dependent high-resolution neutron powder diffraction in the HRPT diffractometer at PSI to address the origin of magnetization reversal at low temperature. The solid solution $Tb_{0.55}Sr_{0.45}MnO_3$ crystallizes in O′ type orthorhombic structure having the Pnma symmetry. The substitution of the divalent cation of Sr^{2+} at the site of Tb^{3+} dilutes the Mn–Tb interaction and affects the magnetic structure, which was observed by the field and temperature-dependent *dc* magnetization and neutron diffraction study. The temperature-dependent zero field-cooled and field cooled *dc* magnetization study reveals the indication of spin reversal phenomena, which is the nature of canted antiferromagnetic or ferrimagnetic transition at 100 Oe because of Mn–Mn sub-lattices interaction below 65 K. By increasing the applied magnetic field up to 20 kOe, a weak ferromagnetic type of behaviour is observed. The field-dependent magnetization shows weak coercivity due to the canted spin structure at low temperatures. The low-temperature neutron diffraction study of polycrystalline $Tb_{0.55}Sr_{0.45}MnO_3$ reveals the non-collinear canted antiferromagnetic structure due to Tb ordering at 1.5 K, which turns into a non-collinear ferromagnetic structure along with spin canting followed by the spin reversal phenomena at 25 K.

1. Introduction

Manganites have always attracted the research interest due to their rich interplay between spin, charge, and orbital ordering, which was revitalized after the discovery of magnetic field controllable ferroelectricity in multiferroic $TbMnO_3$ [1–3]. The single-phase rare-earth manganites $RMnO_3$ and alkaline-earth metal-doped mixed-valent rare-earth manganites $R_{1-x}AE_xMnO_3$ (R = a trivalent rare-earth ion; AE = Alkaline earth metals) are appealing because of their strongly competing magnetic interaction and physical properties such as metal-insulator transition, magneto-resistance and charge ordering [4–6]. The rare-earth manganites without any hole doping (x = 0 and x = 1) are antiferromagnetic and insulating in nature [7]. The magnetic structure of the compounds obtained after substituting the rare-earth ion (R^{3+}) in rare-earth manganites with divalent ion (A^{2+}) may be either ferromagnetic (FM), induced by double exchange (DE) interaction, or antiferromagnetic (AFM) induced by super-exchange (SE) interaction [8]. A non-collinear magnetic structure is then predictable for mixed-valence manganites systems, due to significant competition between double exchange and super-exchange interactions. Also, the replacement of the rare-earth ion with divalent cation leads to a canted spin structure, which further tends to become fully ferromagnetic [9,10].

Most of the research studies related to the mixed-valence manganites are focused on the physical property characterization and magnetic structure study for larger rare-earth ions (R = La, Pr, Nd) [11–13]. There are currently only a few studies on the neutron diffraction and magnetic transition analysis of the mixed-valence manganites when the parent compound is multiferroic (R = Gd,

* Corresponding author.
** Corresponding author.
E-mail addresses: harshit.physics@gmail.com, harshit.agarwal@bhu.ac.in (H. Agarwal), shaz2001in@yahoo.com (M.A. Shaz).

https://doi.org/10.1016/j.jallcom.2020.156355
0925-8388/

Tb, Dy, etc.). Gadolinium is a neutron absorber due to its highest thermal cross-section of any natural element [14] so it is not easy to understand the magnetic structure of the Gd based compound using the neutron diffraction analysis. Alkaline-earth metal-doped rare-earth manganites with larger rare-earth ions have a broader range of average ionic radii and variance in ionic radii, which affect the physical properties of rare-earth manganites. Such properties may also be affected by the doping level of alkaline-earth metal at the A site of rare-earth manganites and distributed in various categories based on one-electron bandwidth 'W' [15,16]. Among the substitution level, the region near the half doping of AE metals shows charge and orbital ordered phase transitions with interesting physical properties [17]. A global phase diagram for the doping level of x = 0.45 for rare-earth manganites from La to Gd is observed based on the variation of ionic radii and the average radius of A site in $R_{0.55}AE_{0.45}MnO_3$ (R = La–Gd, AE = Ca, Sr, Ba) [18]. The magnetic structure analysis by neutron diffraction study of $Tb_{0.55}AE_{0.45}MnO_3$ (AE = Sr, Ca, Ba) is an attention-grabbing area of research.

Multiferroic $TbMnO_3$ with orthorhombic symmetry possesses a distorted structure having magnetic phase transitions, from paramagnetic to an incommensurate antiferromagnetic ordering transition at T_N (41–42 K), and a transition into a multiferroic spin spiral state at T_C (26–28 K), at which a ferroelectric order takes place [19]. A structural correlation to the ferroelectric nature of $TbMnO_3$ at a low temperature of 25 K was observed, which suggests that ferroelectricity is driven by a phase transition from the centrosymmetric orthorhombic structure to a non-centrosymmetric orthorhombic structure via displacement of Mn and O ions, even though the overall orthorhombic symmetry is maintained [20]. A detailed neutron scattering study of Sr-doped Tb-based rare-earth manganite with composition $(Nd_{1-x}Tb_x)_{0.55}Sr_{0.45}MnO_3$ indicates the features of long-range and short-range magnetic ordering in the intermediate region of doping. Also, it shows the feature of long-range C - type canted ferromagnetic metallic case for $x \leq 0.5$ and changes into an insulating state of short-range ferromagnetic and C- or A-type antiferromagnetic state for $x \geq 0.6$ [21]. The Sr^{2+} and Ca^{2+} divalent cation doping at the trivalent Tb site of multiferroic $TbMnO_3$ plays a significant role in changing the magnetic phase transition and the physical properties at low temperatures. The large ionic size mismatch variation at the A site favors the frustration in the ferromagnetic and antiferromagnetic coupling, which leads to spin glass behavior at low temperatures [22,23]. The ferroelectricity and effect of spin reversal have been observed in polycrystalline $Dy_{1-x}Sr_xMnO_3$ [24]. Recently, the evidence for ferromagnetic clusters has been observed at room temperature in Dy and Mn site co-substituted compounds [25].

In the present study, we have doped the Sr at the Tb site of polycrystalline $Tb_{1-x}Sr_xMnO_3$ and observed the magnetic phase transition for x = 0.45. The magnetic structure analysis at low temperatures down to 1.5 K is observed by neutron powder diffraction (NPD). This is complemented by a structural and magnetic study of polycrystalline $Tb_{0.55}Sr_{0.45}MnO_3$ by using the x-ray diffraction and DC magnetization.

2. Experimental

2.1. Synthesis of polycrystalline $Tb_{0.55}Sr_{0.45}MnO_3$

We have synthesized polycrystalline Sr-doped $Tb_{0.55}Sr_{0.45}MnO_3$ (TSMO) by following the conventional solid-state route in a high-temperature programmable furnace. A stoichiometric proportion of high purity (≥99.9% or better) oxide precursors of Tb_4O_7, $SrCO_3$, and MnO_2 powders were placed in a furnace at 150 °C for 24 h preheating. After the preheating process, the precursors are mixed in agate mortar and ground for 8 h. Then the mixture was placed in an alumina boat and calcined at 1250 °C for 24 h. For homogeneity and single-phase formation, the calcined sample is again ground for 2 h and pelletized by applying 6-ton pressure for 20 min. The pellet was sintered at 1350 °C for 24 h followed by furnace cooling. The sintered sample was used for further experiments.

2.2. Structural and microstructural characterization

The synthesized sample has been characterized by X-ray diffraction (XRD) to confirm the crystallinity and phase purity. During the synthesis process, we have observed the XRD for the powder sample two times; one is for the calcined sample at 1250 °C and another one for the sintered sample at 1350 °C. The XRD pattern of the synthesized sample was further analyzed by the Rietveld refinement technique to determine the crystal structure of the sample using the program JANA2006 [26]. The XRD data has been collected with a Panalytical Empyrean X-ray diffractometer at 0.02° 2θ step size in 2θ range from 10° –110°. The microstructure analysis of TSMO was done by using a scanning electron microscope (SEM) using the secondary electron imaging detector and bright field imaging of a high-resolution transmission electron microscope (TEM) operated at 200 kV. The elemental analysis was done by energy dispersive X-ray analysis (EDAX) attached with SEM, which confirms the proper stoichiometry of TSMO.

2.3. Magnetic characterization

The temperature-dependent DC magnetization study has been carried out in the temperature range 2–300 K in Zero-field cooled (ZFC), field cooled cooling (FCC) and then field cooled warming (FCW) mode at 100 Oe, 5000 Oe, 10 kOe and 2 kOe using a quantum design SQUID VSM (70 kOe). Also, the DC Magnetization study of polycrystalline $Tb_{0.55}Sr_{0.45}MnO_3$ sample has been measured as a function of applied magnetic field M(H) (−70 kOe to 70 kOe at different temperatures) by SQUID-VSM (M/s. Quantum design, USA).

2.4. Neutron diffraction study

Neutron diffraction is the best tool to determine the magnetic structure with long-range magnetic ordering. Since the mechanism of neutron scattering depends on the scattering length of the constituent elements in the compound, it is useful to provide accurate information of the atomic positions in the nuclear structure [27]. We have carried out temperature-dependent neutron diffraction on polycrystalline $Tb_{0.55}Sr_{0.45}MnO_3$ at High-Resolution Powder Diffractometer for Thermal Neutrons (HRPT) [28] in the SINQ spallation source at PSI, Switzerland. The sample was filled in a vanadium can; a collection time of 3 h was required for each temperature, ranging from 295 K down to 1.5 K. The wavelength was 1.494 Å. The analysis of nuclear and magnetic refinement is performed by using the program Fullprof [29,30]. The magnetic propagation vector and corresponding irreducible representations were determined by using K-search and BASIREPS modules in Fullprof suite from the peak positions of the magnetic diffraction lines [31].

3. Result and discussion

3.1. Structural characterization of $Tb_{0.55}Sr_{0.45}MnO_3$

$TbMnO_3$ exhibits an orthorhombic crystal structure showing a multiferroic nature. We have replaced the Tb site (Tb^{3+} ion) with Strontium (Sr^{2+}, a divalent cation). The substitution of Sr changes

the Mn oxidation state from Mn^{3+} to Mn^{4+} by doping with Sr^{2+}. The divalent doping in rare-earth manganites induces interesting properties. Intermediate-range hole-doped polycrystalline $Tb_{0.55}Sr_{0.45}MnO_3$ has been successfully obtained by solid-state synthesis. We have analyzed of Sr-doped $TbMnO_3$ by XRD and found a single-phase polycrystalline perovskite oxide. Fig. 1(a) shows the comparison of XRD analysis of calcined TSMO at 1250 °C and sintered TSMO at 1350 °C. After sintering, the Bragg reflections are sharper and well defined, as shown in the inset of Fig. 1 (a). The Rietveld refinement from XRD data of polycrystalline $Tb_{0.55}Sr_{0.45}MnO_3$ is illustrated in Fig. 1(b), which shows that $Tb_{0.55}Sr_{0.45}MnO_3$ crystallizes in the orthorhombic Pnma space group; a view of the crystal structure is shown in Fig. 1(c). Fig. 1(d) shows an octahedral distortion in TSMO having the $a^-b^+a^-$ type Glazer distortion for Pnma. The Mn—O octahedron is slightly distorted from cubic to orthorhombic symmetry. With respect to $TbMnO_3$ structural parameters [20], the lattice parameters of TSMO evolve to a quasi-tetragonal lattice, since the unit-cell parameter 'a' is nearly equal to 'c'. In this way, TSMO possesses the O′ type of lattice distortion, characterized by a lattice arrangement $a \geq c \geq b/\sqrt{2}$, in contrast with the case of the O type of lattice distortion, where the lattice parameter arrangement is $a \geq b/\sqrt{2} \geq c$. So, the orthorhombic structure of TSMO is less distorted than the crystal structure of pure $TbMnO_3$. The refined lattice parameters and atomic coordinates determined from the XRD refinement study are shown in Table 1a, and b respectively.

Since, the properties of the manganites can be tuned by using two main parameters, which are the average ionic radii at the A site $< r_A >$, and the variance of the ionic radii σ^2. In the case of $R_{0.55}AE_{0.45}MnO_3$, the variance σ^2 and average radii of A-site are studied for understanding the magnetic phase transition of the sample [17,18]. Since the Tb/Sr atoms are surrounded by nine oxygen atoms, the values of Shannon ionic radii for nine-fold coordination are considered. The average radius of the A-site $< r_A >$ ($Tb_{0.55}/Sr_{0.45}$) in $Tb_{0.55}Sr_{0.45}MnO_3$ is 1.192 Å and variance of the ionic radii σ^2 is 0.011. The phase diagram having the effect of average radius and variance of ionic radii was observed for the rare-earth manganites from La to Gd. It is expected from the phase diagram that $Tb_{0.55}Sr_{0.45}MnO_3$ must have an intermediate behavior between the insulating spin-glass structure and ferromagnetic metallic state [21].

The Microstructural study of the TSMO has been carried out by the scanning electron microscopy (SEM) and Transmission electron microscopy (TEM). Fig. 2(a) shows the secondary electron imaging of the TSMO sintered sample coated by platinum, which shows the chunks of polycrystalline TSMO. As the sintered pellet is crushed and ground in an agate mortar pestle, so the particles are varying in size and show the homogeneous solid solution of TSMO. However, the average crystallite size of the sample is 60 nm observed using the XRD characterization. The Energy dispersive X-ray analysis coupled with SEM shows the presence of Sr, Tb, Mn, and O in the sample shown in Fig. 2 (b). For further microstructural

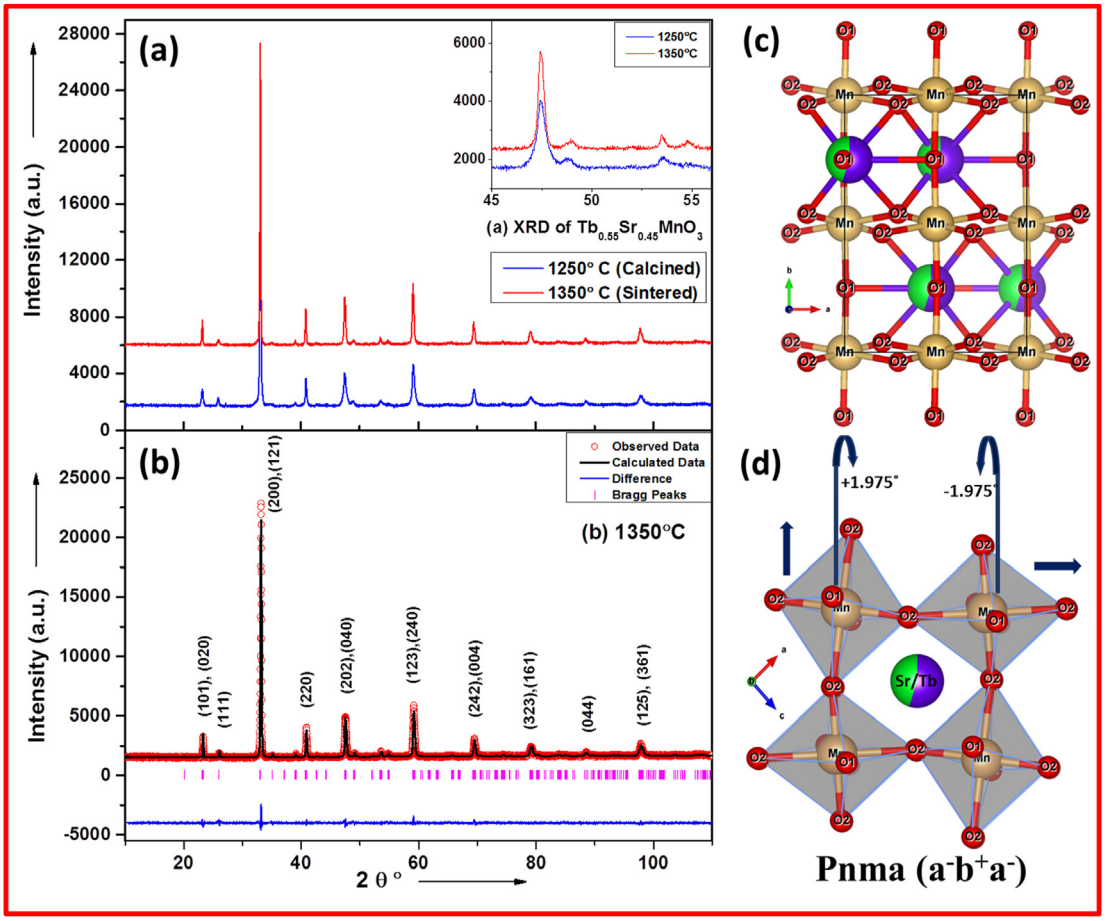

Fig. 1. (a) Comparison of XRD analysis of calcined $Tb_{0.55}Sr_{0.45}MnO_3$ at 1250 °C (blue color) and sintered $Tb_{0.55}Sr_{0.45}MnO_3$ (TSMO) at 1350 °C (red color) with inset showing the clear changes in XRD data in between the 2 θ range for 45° to 57°; **(b)** Rietveld refinement of X-ray Diffraction data of polycrystalline TSMO synthesized at 1350 °C; **(c)** Orthorhombic structure having the centrosymmetric Pnma space-group; **(d)** Octahedral distortion in Pnma symmetry with $a^-b^+a^-$ Glazer notation. (For interpretation of the references to color in this figure legend, the reader is referred to the Web version of this article.)

Table 1a
Lattice Parameters and Structural refinement parameters for TSMO observed by XRD.

Refined Parameters and Phase Data	
Unit-Cell Parameters	a = 5.421(7) Å, b = 7.629(3) Å, c = 5.406(9) Å, $\alpha = \beta = \gamma = 90^{\circ}$
Space Group	Pnma (Centrosymmetric)
R- Factor	R_p = 1.93%, R_{wp} = 2.55%, GOF = 1.06%, R_{Bragg} = 3.94%, wR_{Bragg} = 3.75%
Volume	V = 223.65(3) $Å^3$

Table 1b
Atomic Parameters for TSMO at room temperature.

Atoms	Atomic Positions			U_{iso} Factor	Wyckoff position	Occupancy
	x	y	z			
Tb	0.9744(3)	0.25	0.0078(5)	0.005	4c	0.55
Sr	0.9744(3)	0.25	0.0078(5)	0.005	4c	0.45
Mn	0.5	0	0	0.001	4b	1
O1	0.0073(4)	0.25	0.5679(2)	0.008	4c	1
O2	0.7061(6)	0.4622(6)	0.2515(9)	0.001	8d	1

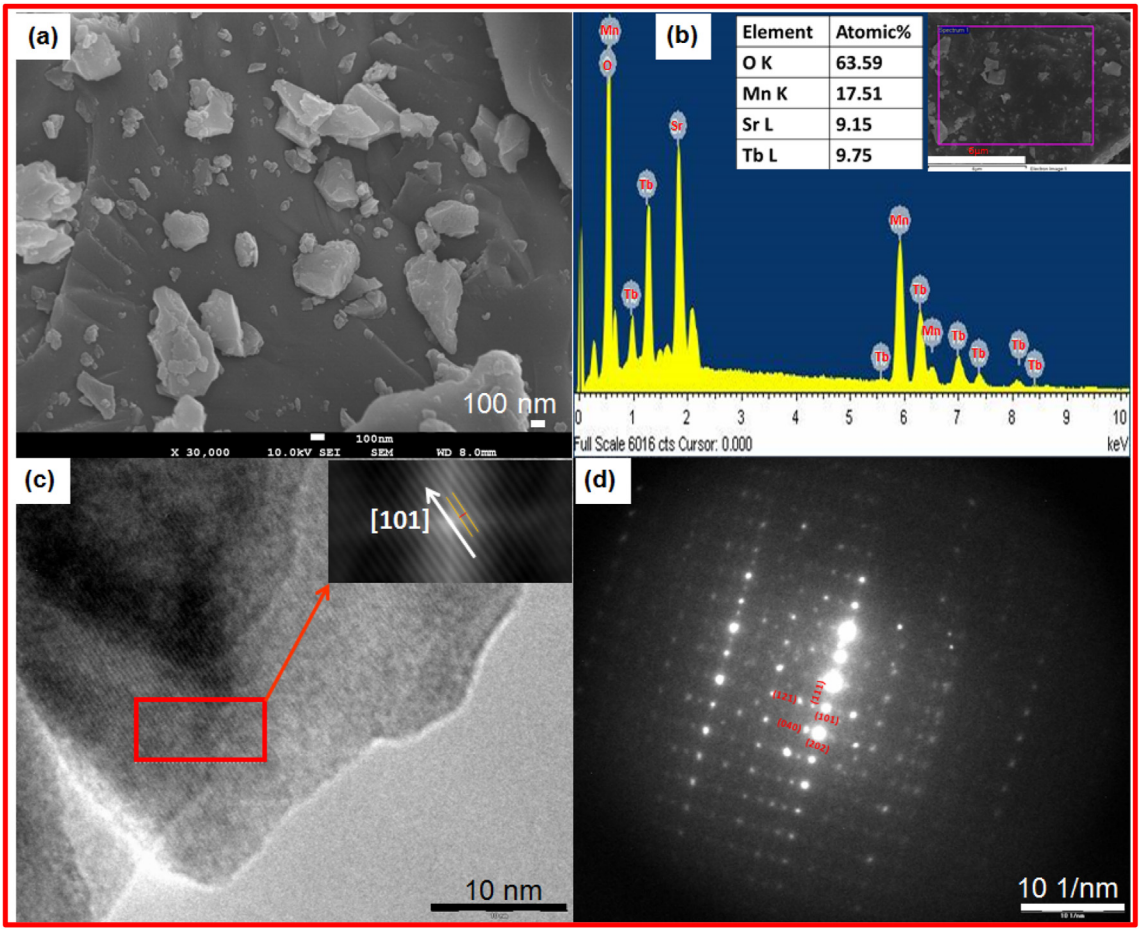

Fig. 2. (a) Surface morphology of polycrystalline TSMO coated by Platinum, which is observed by secondary electron imaging of SEM; **(b)** Energy dispersive X-ray analysis of synthesized sample; **(c)** High resolution lattice fringe imaging (HRLFI) observed by high resolution Transmission electron microscope; the inset displays the Fourier filtered HR-LFI showing the interplaner spacing aligned along the [101] direction; **(d)** SAED pattern indexed for polycrystalline TSMO having Pnma symmetry.

characterization, we have observed the bright field imaging of TSMO by TEM, showing interesting features of polycrystalline TSMO. Fig. 2(c) shows the High-resolution lattice fringe imaging (HRLFI) observed by high-resolution TEM in bright field mode. The inset displays the Fourier filtered HR-LFI, which is filtered by the Gatan Microscope tool. The interplanar spacing is 3.92 Å, which means that the crystal is arranged in [101] direction. Fig. 2(d) shows the SAED pattern for TSMO at 10 1/nm scales, which is confirming the single-phase character of orthorhombic TSMO.

3.2. Magnetic characterization of $Tb_{0.55}Sr_{0.45}MnO_3$

We have measured the magnetic properties at various temperatures down to 5 K and field up to 70 kOe. Fig. 3 (a) shows the temperature-dependent DC magnetization study in which the system was cooled down to 5 K. Then a magnetic field of 100 Oe was applied and magnetization data were collected up to 300 K, which is the zero-field cooled (ZFC) state shown in Fig. 3(a) as a black colored curve. After applying a field of 100 Oe, the data were collected by cooling the system again down to 5 K, which is known as field-cooled cooling (FCC), depicted as the red curve in Fig. 3 (a). For checking the reversibility in the magnetization curve, the system was again warmed to 300 K and the data was collected, which is known as field-cooled warming state (FCW), depicted by the blue curve in Fig. 3 (a). We have found that during the ZFC state, as we go from 5 K to 300K, the magnetization from the weak saturation starts to decrease to 25 K and then increases to a maximum at T_{cusp}^{ZFC} ~41 K, after which it decreases exponentially up to 300 K. During the field-cooled cooling (FCC) from 300K to 5K, the magnetization curve bifurcates from the ZFC curve at 65 K and increased up to T_{cusp}^{FC} ~ 39 K. The bifurcation temperature is considered to indicate the first transition temperature happening due to Mn ordering, which is visible in the inset of Fig. 3 (b). Also, the bifurcation and irreversibility in the ZFC/FCC data may be the effect of spin reorientation or spin glass nature of the sample but below 40 K, the FCC magnetization is decreased and crossed the ZFC magnetization curve at $T_{SR} = 21$ K, known as spin-reversal temperature. After this, the FCC state comes in the same saturation state of magnetization below $T_{Tb} = 8$ K, which is considered to be another magnetic transition temperature due to Tb ordering. We have not observed any changes in the FCW state and found it to be similar to the FCC state of magnetization. Since the magnetization in the FC state is lower than the ZFC state, it may not be the effect of a spin-glass state [32]. Such type of reversal magnetization phenomena may be the reason for a canted spin structure, due to the formation of two sub-lattices with different coercive fields and different magnetization behavior, which generally happens in ferrimagnetism. The temperature-dependent inverse susceptibility is obtained from the ZFC mode at 100 Oe shown in Fig. 3 (c) and fitted by the Curie-Weiss law in the temperature range of 100 K–300 K {$\chi = C/(T - \theta)$, where C is Curie Constant, and θ is Weiss temperature}, which also indicates the weak ferromagnetic with canted spin or ferrimagnetic behavior of polycrystalline TSMO at low temperature. Such type of ferrimagnetism and spin reversal phenomena has also been observed in (Gd, Ca)MnO_3 [33]. The experimentally observed effective magnetic moment of polycrystalline TSMO is 10.76 μ_B, which is close to the theoretical value of the effective magnetic moment (TSMO μ_{eff} = 8.476 μ_B, the square root of the sum of theoretical moments as 0.55 $(\mu Tb^{3+})^2$ + 0.55 $(\mu Mn^{3+})^2$ + 0.45 $(\mu Mn^{4+})^2$ where $\mu_{Tb3+} = 9.72\mu_B$, $\mu_{Mn3+} = 4.89\mu_B$, $\mu_{Mn4+} = 3.87\mu_B$). Also, the Curie constant (C) and Weiss temperature (θ) for polycrystalline TSMO are 14.482 emu K- Oe^{-1}. mol^{-1} and 14.884 K respectively, which is positive in nature. To investigate the irreversible magnetization (IRM) [34], the difference between FC and ZFC curves, $M_{IRM} = M_{FC} - M_{ZFC}$ is plotted in Fig. 3(d). M_{IRM} shows a negative value under the low magnetic field (100 Oe) in a certain temperature region. This unusual feature may be related to the large magneto-striction present in this material. The mechanism of magneto-striction originates from the interchange coupling of the magnetic moments of atoms in the sample below 21 K.

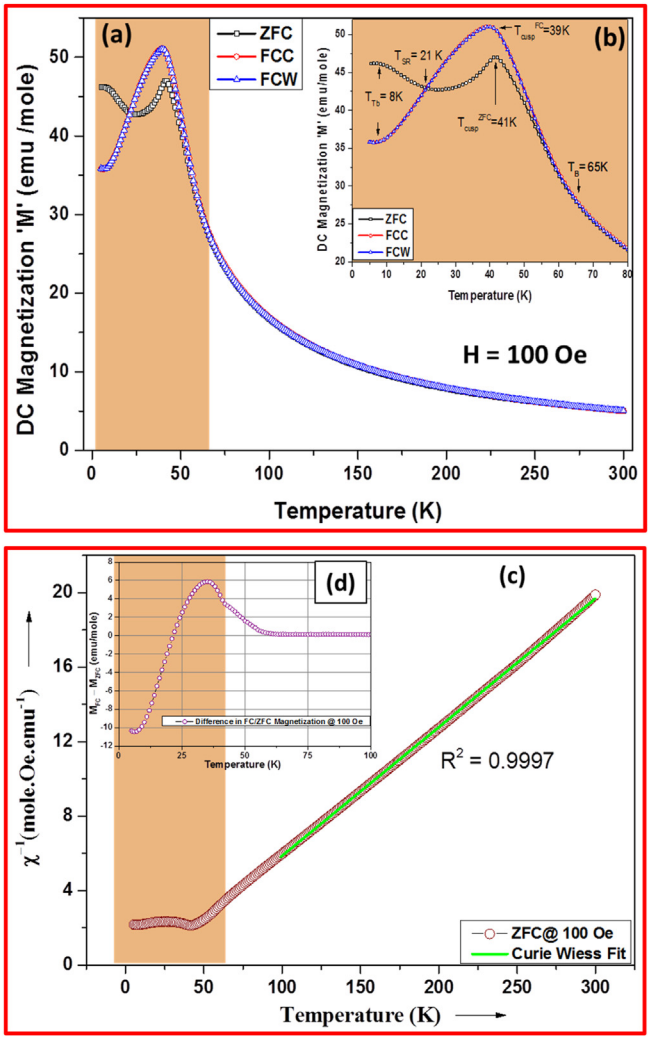

Fig. 3. (a) The Temperature-dependent Zero Field Cooled, Field-Cooled Cooling, and Field- Cooled Warming DC magnetization study of polycrystalline TSMO observed at 100 Oe; **(b)** the inset is showing the bifurcation in ZFC and FCC/FCW curve at T_B ~ 65 K, related to the Mn ordering temperature; the spin reversal transition due to Mn–Mn sublattice interaction and canted antiferromagnetic transition due to Tb^{3+} ion at T_{Tb} ~ 8 K; **(c)** Inverse susceptibility study obtained by ZFC curve with Curie-Weiss Fitting having the linearity parameter R^2 = 0.9997, showing the weak ferromagnetic with canted spin or ferrimagnetic nature of the sample; **(d)** Irreversible magnetization related to the magneto-striction present in the polycrystalline TSMO.

For reconfirmation of the DC magnetization behavior, we have performed the temperature-dependent DC magnetization study on various fields, which are 100 Oe, 5000 Oe, 10 kOe and 20 kOe in the temperature range 5 K–100 K; shown in Fig. 4 (a), (b), (c) and (d) respectively. Also, the temperature-dependent inverse susceptibility is plotted in the same graph on another Y-axis. The spin reversal effect of magnetization at low temperatures seems to violate by increasing the magnetic field. We have observed that the effect of magneto-striction has been changed by applying the magnetic field.

Fig. 5 shows the field-dependent DC magnetization curve M (H) for polycrystalline TSMO collected in between the magnetic field of ±70 kOe, at various temperatures 5 K, 25 K, 60 K, 100 K, and 300 K. We have observed that there is no saturation in the field-dependent magnetization curve down to 5 K. Also, a weak coercivity of ~2810 Oe and ~700 Oe are observed at 5 K and 25 K respectively, which may be the effect of canted spins or the ferrimagnetic nature of the sample. For confirming the magnetic structure of the polycrystalline TSMO, our further study is focused on the Neutron Diffraction experiments.

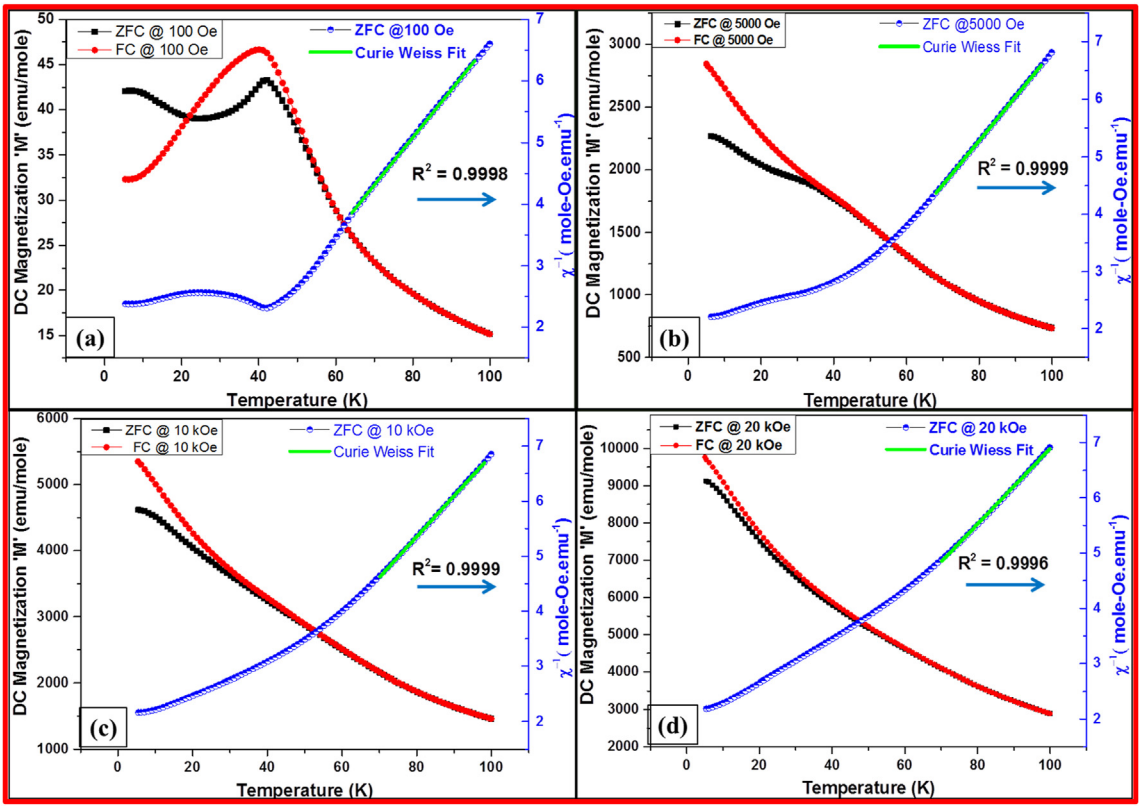

Fig. 4. Temperature-dependent DC magnetization of polycrystalline TSMO along with the inverse susceptibility at **(a)** 100 Oe; **(b)** 500 Oe; **(c)** 10 kOe; **(d)** 20 kOe, in the temperature range of 5K−100K.

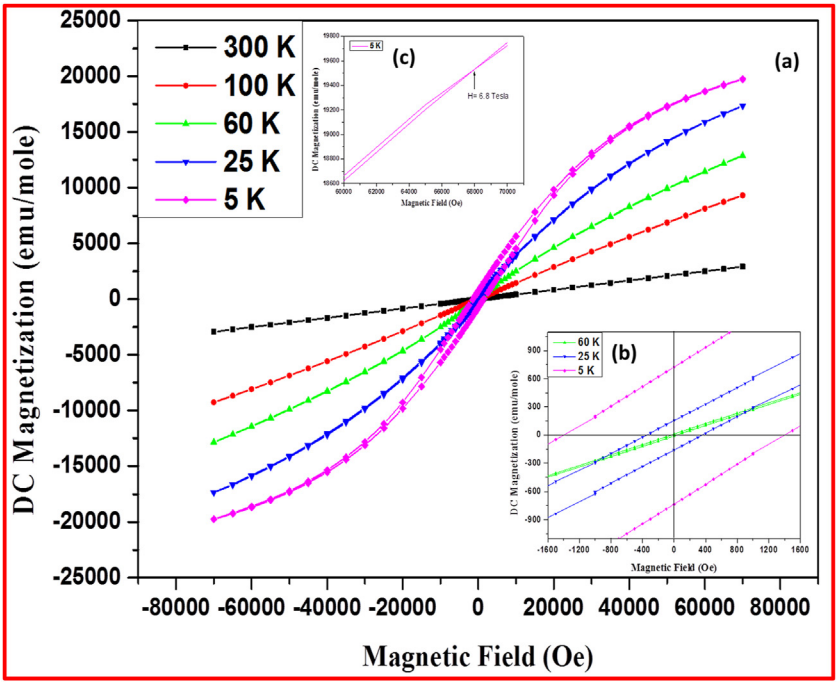

Fig. 5. **(a)** Field dependent DC magnetization M − H behavior of polycrystalline TSMO at various temperatures down to 5K and magnetic field −70 kOe to +7 kOe; **(b)** inset is showing the weak coercivity at 25 K and 5 K; **(c)** the M/H loop is further opening at 6.8 kOe without following any saturation.

3.3. Neutron diffraction study of $Tb_{0.55}Sr_{0.45}MnO_3$

The magnetic structure of the orthorhombic $TbMnO_3$ parent compound was found to be spiral antiferromagnetic as per the neutron diffraction study [19]. When the rare-earth ion was partially substituted by an alkaline earth metal having a divalent state, the antiferromagnetic phase becomes distorted and transforms into a canted structure before becoming fully ferromagnetic [9]. The magnetic structure is expected to be transformed for the substitution of alkaline-earth metal; the introduction of Sr^{2+} has changed the Mn state to a mixed-valent state and it has also diluted the magnetic contribution of Tb^{3+} ion. For the study of the magnetic structure of $Tb_{0.55}Sr_{0.45}MnO_3$, neutron powder diffraction (NPD) patterns at different temperatures of 300 K, 150 K, 50 K, 25 K, and 1.5 K have been acquired. The observed neutron diffraction patterns at various temperatures are depicted in Fig. 6, and the inset shows the important low-angle 2θ regions. We can observe that there is no signature of any additional peak down to 150 K, and at 50 K a feeble hump-like feature around $2\theta = 15.8^{\circ}$ starts appearing. As the temperature decreases, the new peak develops from this hump-like feature. This situation points out towards an interesting magnetic structure, which will be discussed further in the text. The nuclear structure at all the temperatures has been refined by the Rietveld method from the NPD patterns, using the program Fullprof. The temperature dependent variation in lattice structural parameters and refined phase data along with the Mn−O − Mn bond angle and bond length has been observed from the nuclear structure refinement of NPD patterns, which is mentioned in Table 2. The variation in these parameters is visible in Fig. 7**.** A small anomaly in the Mn−O distances at the phase transition is expected. The signification of this study is to show how the Mn−O distances and lattice parameters are changing by decreasing the temperature. Nevertheless, the symmetry of the lattice is maintained from 300 K to 1.5 K, which is orthorhombic in all T range. Table 3 represents the temperature-dependent variation of the atomic position of Tb/Sr, Mn and Oxygen atoms. At all temperatures, TSMO follows the condition of $a \geq c \geq b/\sqrt{2}$, which shows that the TSMO is maintaining its centrosymmetric symmetry of O′ type with Pnma structure down to 1.5 K.

Table 2
Neutron powder diffraction refinement parameters of polycrystalline TSMO at various temperatures down to 1.5 K

Parameters	300 K	150 K	50 K	25 K	1.5 K
a (Å)	5.411(3)	5.410(6)	5.409(5)	5.409(1)	5.408(6)
b (Å)	7.626(4)	7.616(2)	7.611(5)	7.610(5)	7.611(2)
c (Å)	5.398(2)	5.394(5)	5.392(9)	5.392(8)	5.392(3)
b/√2 (Å)	5.393(2)	5.386(3)	5.383(1)	5.382(2)	5.382(7)
Mn−O1/Mn−O4 (Å)	1.940(4)	1.937(5)	1.936(1)	1.936(1)	1.936(8)
Mn−O2/Mn−O5 (Å)	1.934(2)	1.932(1)	1.930(2)	1.935(7)	1.936(3)
Mn−O3/Mn−O6 (Å)	1.949(9)	1.952(9)	1.955(2)	1.947(8)	1.949(1)
Mn−O1−Mn ()	158.53(3)	158.67(5)	158.74(9)	158.64(9)	158.46(9)
Mn−O2−Mn ()	159.42(5)	159.04(3)	158.82(4)	159.08(9)	158.75(3)
Volume ($Å^3$)	222.76(3)	222.30(4)	222.05(8)	222.03(1)	221.91(5)
Bragg R-factor (%)	1.68(8)	1.57(3)	1.80(8)	2.02(5)	1.67(4)
R_f factor (%)	1.18(1)	1.21(7)	1.25(7)	1.28(6)	1.13(4)
Chi Square	1.68	1.74	2.10	2.10	2.14
Magnetic R factor	–	–	39.6	28.58	14.61

The magnetic contribution in NPD patterns due to long-range ordering of Mn moments was found to start at 50 K, which continues down to 1.5 K. After the nuclear structure refinement of TSMO, the magnetic propagation was analyzed by following the K-search program. As discussed aforementioned in Fig. 6, in the NPD patterns acquired at T = 25 K and T = 1.5 K, a new Bragg peak around $2\theta = 15.8^{\circ}$ is observed, which can be indexed as (1, 0, 0) + (0, 0, 1). This Bragg peak is forbidden for the Pnma space group and it comes from the ordering of the Mn sublattice. It indicates that the magnetic ordering is characterized by the propagation vector **k** = (0,0,0). For the space group Pnma, the little group $\Gamma_{\mathbf{K}}$ formed with the elements that leave **k** invariant coincides with the space group. The irreducible representations calculated from the program BASIREPS for the magnetic symmetry analysis areas are presented in Table 4:

The spatial notation for the magnetic atoms is:

Mn (site 4b): **1** (0, 0, 1/2); **2** (1/2, 0, 0); **3** (0, 1/2, 1/2); **4** (1/2, 1/2, 0)

Tb (site 4c): **5** (0.9686, 0.25, 0.0049); **6** (−0.4686, −0.25, 0.5049) **7** (−0.9686, 0.75, −0.0049); **8** (1.4686, 0.252, 0.4951)

According to group theory, the possible solutions for these

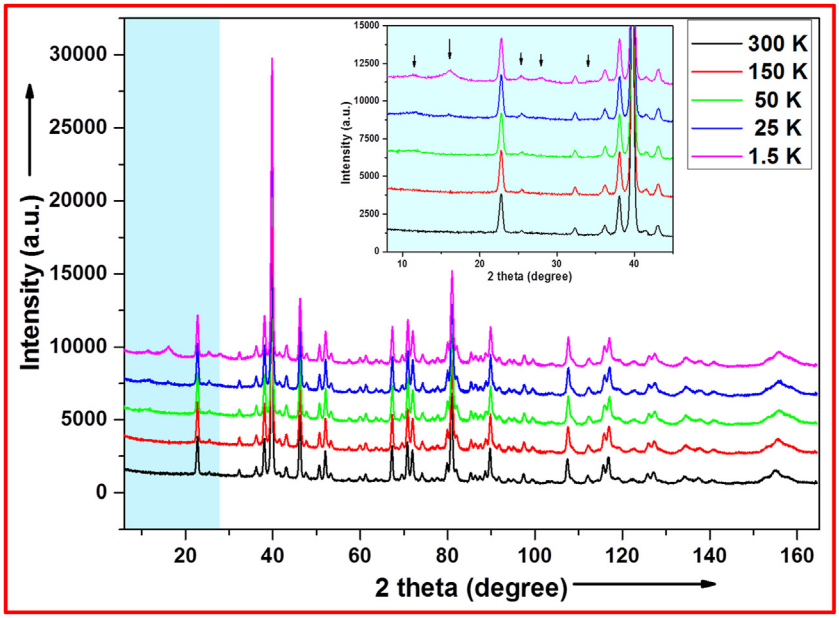

Fig. 6. Neutron Powder Diffraction Study of polycrystalline TSMO at 300 K, 150 K, 50 K, 25 K, and 1.5 K. Inset is showing the changes observed in NPD patterns.

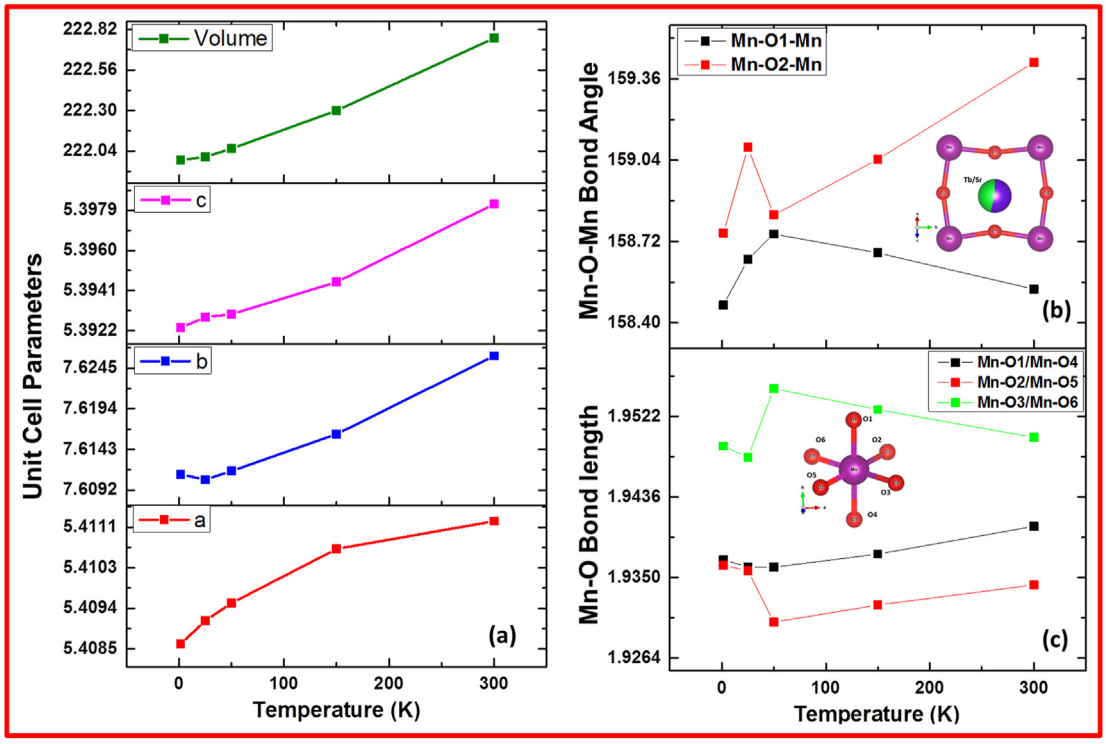

Fig. 7. Variation in Crystallographic parameters observed by NPD of polycrystalline TSMO at various temperatures **(a)** Unit cell parameter **(b)** Mn−O − Mn Bond angle **(c)** Mn−O Bond Length.

Table 3
Refined structural variation in polycrystalline TSMO observed form Rietveld refinement of neutron powder diffraction patterns.

		300 K	150 K	50 K	25 K	1.5 K	Site
Tb	**x**	0.9701(5)	0.9695(4)	0.9690(6)	0.9695(8)	0.9685(6)	4c
	y	0.25	0.25	0.25	0.25	0.25	
	z	0.0004(9)	0.0039(8)	0.0037(1)	0.0044(7)	0.0049(3)	
	U	0.01	0.008	0.005	0.005	0.005	
Sr	**x**	0.9701(5)	0.9695(4)	0.9690(6)	0.9695(8)	0.9685(6)	4c
	y	0.25	0.25	0.25	0.25	0.25	
	z	0.0004(9)	0.0039(8)	0.0037(1)	0.0044(7)	0.0049(3)	
	U	0.01	0.008	0.005	0.005	0.005	
Mn	**x**	0.5	0.5	0.5	0.5	0.5	4b
	y	0	0	0	0	0	
	z	0	0	0	0	0	
	U	0.009	0.007	0.007	0.006	0.006	
O1	**x**	0.0128(9)	0.0130(5)	0.0130(4)	0.0116(6)	0.0138(4)	4c
	y	0.25	0.25	0.25	0.25	0.25	
	z	0.5656(9)	0.5651(5)	0.5648(9)	0.5654(7)	0.5656(4)	
	U	0.016	0.017	0.014	0.015	0.014	
O2	**x**	0.7190(7)	0.7183(6)	0.7181(3)	0.7190(4)	0.7180(5)	8d
	y	0.4658(4)	0.4650(1)	0.464(3)	0.4650(4)	0.4648(7)	
	z	0.2789(8)	0.2790(4)	0.2787(3)	0.2795(3)	0.2804(4)	
	U	0.018	0.019	0.017	0.017	0.016	

Table 4
Irreducible representations: p = 1/2.

	{1|000}	{2_00z|p0p}	{2_0y0|0p0}	{2_x00|ppp}	{-1|000}	{m_xy0|	{m_x0z|0p0}	{m_0yz|ppp}
Γ_1	1	1	1	1	1	1	1	1
Γ_2	1	1	1	1	−1	−1	−1	−1
Γ_3	1	1	−1	−1	1	1	−1	−1
Γ_4	1	1	−1	−1	−1	−1	1	1
Γ_5	1	−1	1	−1	1	−1	1	−1
Γ_6	1	−1	1	−1	−1	1	−1	1
Γ_7	1	−1	−1	1	1	−1	−1	1
Γ_8	1	−1	−1	1	−1	1	1	−1

Table 5
Notation for Mn and Tb ion according to Group theory.

	Mn	Tb
Γ_1	(A_x, G_y, C_z)	(0, G_y, 0)
Γ_2		(A_x, 0, C_z)
Γ_3	(G_x, A_y, F_z)	(G_x, 0, F_z)
Γ_4		(0, A_y, 0)
Γ_5	(C_x, F_y, A_z)	(0, F_y, 0)
Γ_6		(C_x, 0, A_z)
Γ_7	(F_x, C_y, G_z)	(F_x, 0, G_z)
Γ_8		(0, C_y, 0)

Mn	Tb
$F = m_1 + m_2 + m_3 + m_4$	$F = m_5 + m_6 + m_7 + m_8$
$G = m_1 - m_2 + m_3 - m_4$	$G = m_5 - m_6 + m_7 - m_8$
$C = m_1 + m_2 - m_3 - m_4$	$C = m_5 + m_6 - m_7 - m_8$
$A = m_1 - m_2 - m_3 + m_4$	$A = m_5 - m_6 - m_7 + m_8$

magnetic atoms and notation for the basis vectors are mentioned in Table 5.

On the other hand, around 50% of the Tb positions must be occupied by Sr atoms, and probably they are randomly distributed. So it can be considered that the Tb atoms do not contribute to the long-range magnetic order, although a short-range ordering is probable. The magnetic structure factor, if only the Mn is considered is:

$$\vec{F}_M = f\left(|\vec{h}|\right)\left(\vec{m}_1 e^{l\pi i} + \vec{m}_2 e^{h\pi i} + \vec{m}_3 e^{(k+l)\pi i} + \vec{m}_4 e^{(k+k)\pi i}\right)$$

where $f(|\boldsymbol{h}|)$ is the atomic magnetic form factor of Mn. The reflection at $2\theta = 15.8^\circ$ corresponds to the Bragg reflections (1,0,0) + (0,0,1). The magnetic structure factor is:

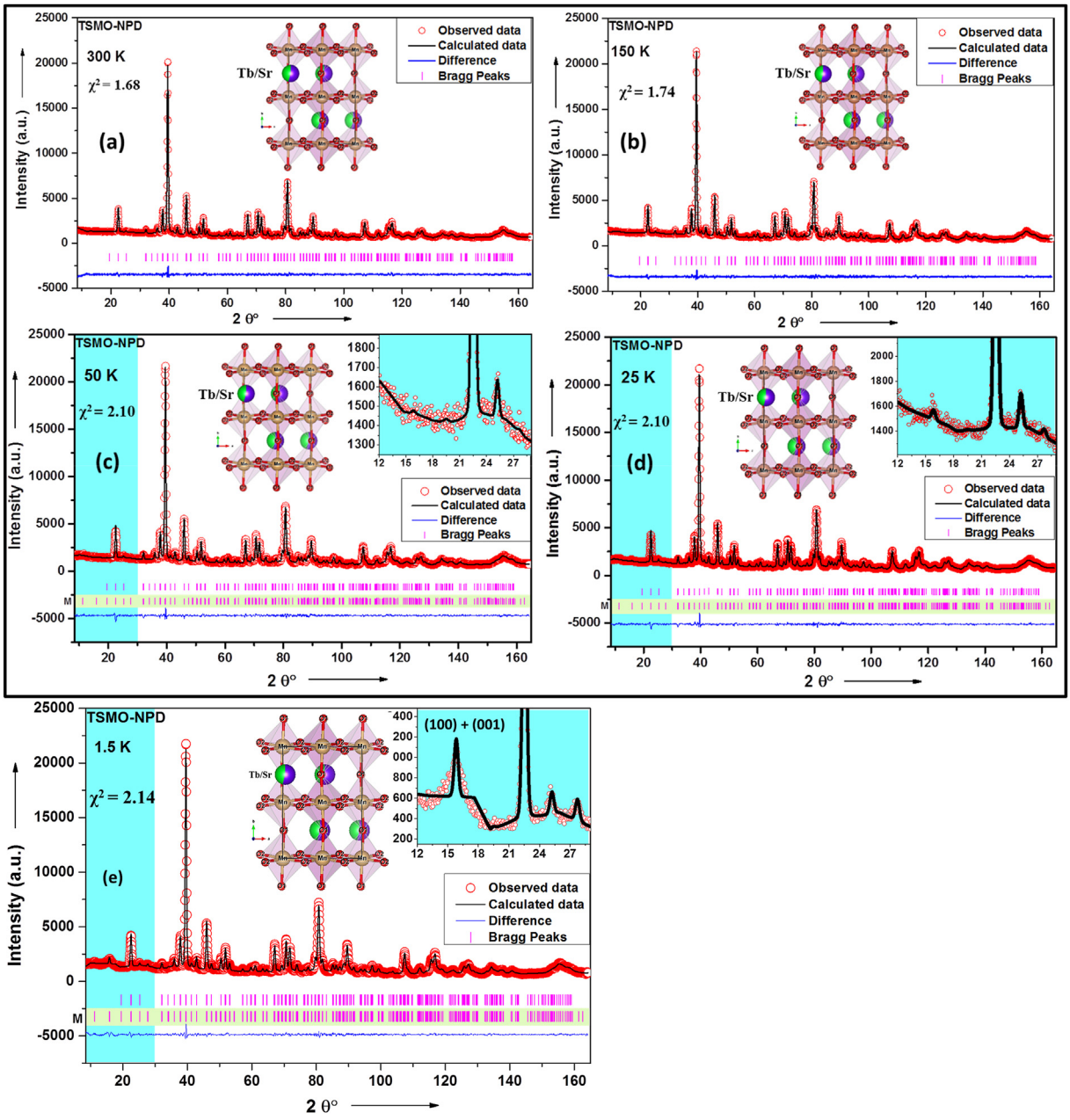

Fig. 8. Neutron Diffraction pattern refinement using Rietveld Analysis along with the nuclear structure having Pnma symmetry at **(a)** 300 K **(b)** 150 K **(c)** 50 K and **(d)** 25 K. Inset of the figure (c) and (d) represent the magnetic peak refinement observed at 15.8° 2 θ. **(e)** Rietveld refinement of Neutron Diffraction pattern along with the nuclear structure at 1.5 K. The inset is showing the diffuse scattering reflection observed at 15.8° 2 θ due to short-range ordering of Tb.

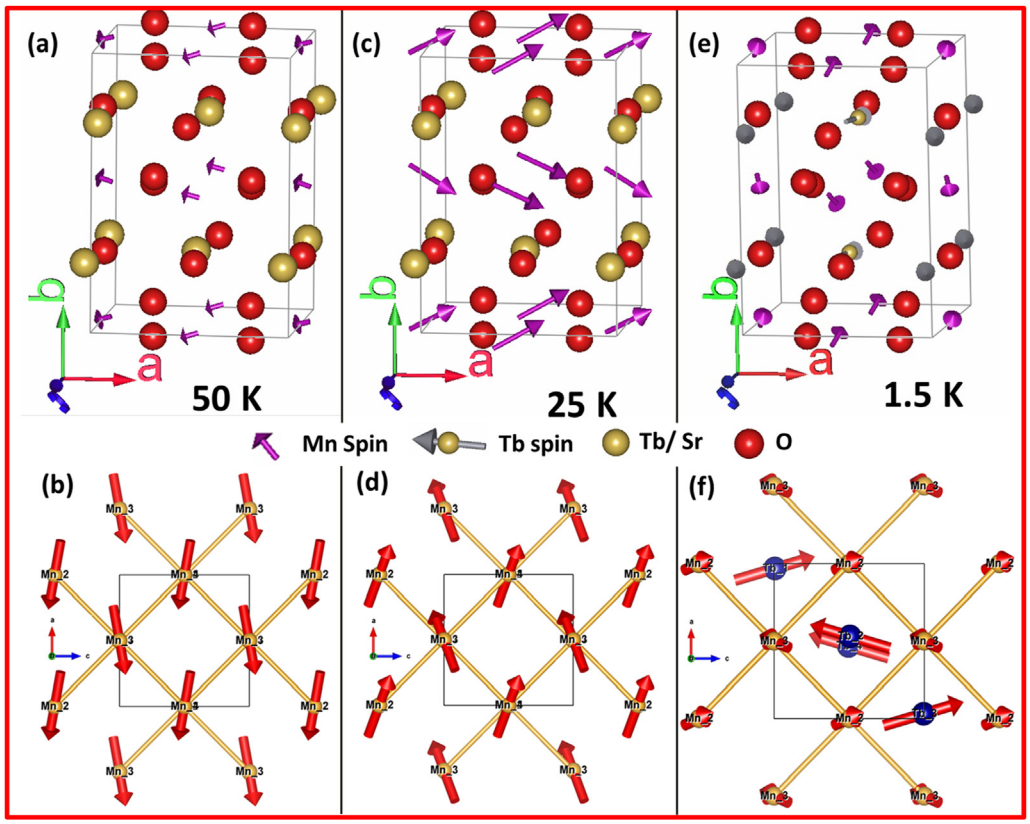

Fig. 9. Magnetic structure of polycrystalline TSMO at **(a, b)** 50 K having large ferromagnetic ordering with weak antiferromagnetic canting of Mn spin in the (−)ve 'a' direction along with the top view of the magnetic lattice **(c, d)** 25 K due to the spin orientation of canted ferromagnetic ordering in the (+)ve 'a' direction along with the top view of the magnetic lattice **(e, f)** 1.5 K due to the non-collinear antiferromagnetic ordering of Tb and Mn spin follows the magnetization reversal along with the top view of magnetic lattice having Tb and Mn spin.

Table 6
Magnetic moment of different cations at various temperatures.

Temperature	Cation	m_x	m_y	m_z	Magnetic Moment
50 K	$Mn^{3+/4+}$	1.25(3)	0.36(9)	−0.22(6)	0.50(7)
25 K	$Mn^{3+/4+}$	1.35(2)	0.71(7)	−0.50(1)	1.61(1)
1.5 K	$Mn^{3+/4+}$	0.22(7)	0.45(4)	−0.52(3)	0.72(9)
	Tb^{3+}	0.41(6)	0	1.43(5)	1.49(4)

$$\vec{F}_M(1,0,0) = k(\vec{m}_1 - \vec{m}_2 + \vec{m}_3 - \vec{m}_4)$$

$$\vec{F}_M(0,0,1) = k(-\vec{m}_1 + \vec{m}_2 - \vec{m}_3 + \vec{m}_4)$$

The magnetic structure factors of the reflections (1,0,0) and (0,0,1) are different from zero only for the basis vector **G.** So, the possible solutions correspond to Γ_1, Γ_3, and Γ_7. The possible solutions correspond to G_3 and G_7 irreducible representations. On the other hand, the magnetization curves give a small ferromagnetic component. It means that there is a canting of the magnetic structure when a magnetic field is applied. So, only the solutions of Γ_3 and Γ_7, which are (G_x, A_y, F_z) and (F_x, C_y, G_z), respectively, are acceptable. Fig. 8 illustrates the Rietveld refinement study from the NPD patterns at (a) 300 K, (b) 150K, (c) 50 K and (d) 25 K. Fig. 8 (e) depicts the refinement of NPD pattern at 1.5 K. The inset displays the presence of a diffuse scattering peak, which may be originated by a short-range ordering of the Tb lattice, with a glassy nature of spin orientation.

The magnetic structure at 50K is a canted ferromagnetic-type structure having the canted spin along the negative a-axis, as shown in Fig. 9 (a, b). According to the spin reversal phenomenon observed in the DC magnetization study, we have found that the spin of Mn atoms in the magnetic structure observed at 25 K follows the spin reversal condition, as the Mn spin is canted along the positive a-axis. The refinement of the magnetic structure in both cases is following the Γ_7 solution, which is (F_x, C_y, G_z) for Mn atom. The spins in each layer are oriented at different angles, which are expected to be happening due to Mn−O−Mn superexchange interactions within the Mn sublattices. Also, the canting in spins leads to some magnetic moment, which was the indication of the ferromagnetic-type nature observed in the DC magnetization study. Fig. 9(c and d) shows the canted ferromagnetic structure along the positive a-axis. The NPD pattern observed at 1.5 K has also been refined using the irreducible representation of Γ_7 solution, which is (F_x, C_y, G_z) for Mn atom and (F_x, 0, G_z) for Tb atom. Such type of non-collinear spin ordered magnetism is well explained in multiferroic perovskites [35]. Table 6 shows the refined coefficient for the resulting magnetic structure.

In addition to this, we have observed the diffuse scattering in the magnetic reflection at $2\theta = 15.8°$, which indicates the short-range ordering of Terbium, as the doping of Sr dilutes the magnetic contribution of Tb moments at low temperature. The Mn−Tb coupling is weaker than the Mn−Mn coupling. The Tb−Tb interaction leads to a canted antiferromagnetic ordering in the magnetic structure observed at 1.5 K, as shown in Fig. 9 (e, f), along with the top view of the magnetic square lattice.

It is clear from the complementary observation of DC magnetization and neutron diffraction that TSMO has a canted-spin

orientation at low temperature, below 65 K. Polycrystalline $Tb_{0.55}Sr_{0.45}MnO_3$ has an orthorhombic structure with the long-range canted ferromagnetic ordering of Mn ions below 65 K, which turns into the short-range antiferromagnetic ordering of Tb ion having F_xG_z type magnetic structure and canted antiferromagnetic ordering of Mn ion having a $F_xC_yG_z$-type magnetic structure below 8 K.

4. Conclusion

Terbium ions with large magnetic moments play a significant role in modulating the magnetic properties of manganites due to Mn−Mn and Mn−Tb lattice interaction. The Sr doping induces a mixed-valent state of Mn^{3+}/Mn^{4+} and dilutes the magnetic interactions of Tb^{3+} ion. DC magnetization study reveals the magnetization reversal phenomena in TSMO, which is happening due to ferrimagnetic or canted spin ordering of Mn−Mn sublattice. The neutron diffraction study confirms the exact location of atomic positions. It also states that TSMO has a long-range canted ferromagnetic ordering at 50 K and 25 K. The magnetic ordering induced a short-range canted antiferromagnetic ordering of Tb ions at 1.5 K.

CRediT authorship contribution statement

Harshit Agarwal: Writing - original draft, Formal analysis, Investigation. **Jose.A. Alonso:** Writing - review & editing, Formal analysis. **Ángel Muñoz:** Writing - review & editing. **R.J. Choudhary:** Investigation. **O.N. Srivastava:** Writing - review & editing. **M.A. Shaz:** Supervision, Writing - review & editing.

Declaration of competing interest

The authors declare that they have no known competing financial interests or personal relationships that could have appeared to influence the work reported in this paper.

Acknowledgments

HA and MAS are obliged to Prof. Anand Chaudhary for providing the high-temperature furnace facility. Authors are gratified to Dr. S. D. Kaushik for providing salient suggestions on the manuscript; and Dr. N. P. Lalla, Dr. Alok Banarjee, Prof. D. Sa, and Prof. A. K. Ghosh for fruitful discussion. 'HA' is thankful to Pooja Pant and Keshav Kumar for their help in research work. Author 'HA' would like to acknowledge the CSIR India for providing senior research fellowship (09/013(0763)/2018-EMR-I). Author 'MAS' is thankful to UGC-DAE CSR and DST-FIST for funding. JAA acknowledges the Spanish MINECO, Spain for funding the project MAT2017-84496-R. We thank the SINQ-PSI facility for proving neutron beam time.

References

[1] M. Fiebig, Revival of the magnetoelectric effect, J. Phys. D Appl. Phys. 38 (2005), https://doi.org/10.1088/0022-3727/38/8/R01.
[2] T. Kimura, T. Goto, H. Shintani, K. Ishizaka, T. Arima, Y. Tokura, Magnetic control of ferroelectric polarization, Nature 426 (2003) 55−58, https://doi.org/10.1038/nature02018.
[3] N. Nagaosa, Multiferroics, in: Spin Curr, 2017, pp. 160−184, https://doi.org/10.1093/oso/9780198787075.003.0010.
[4] T. Goto, Y. Yamasaki, H. Watanabe, T. Kimura, Y. Tokura, Anticorrelation between ferromagnetism and ferroelectricity in perovskite manganites, Phys. Rev. B Condens. Matter 72 (2005), https://doi.org/10.1103/PhysRevB.72.220403.
[5] M. Baldini, T. Muramatsu, M. Sherafati, H.K. Mao, L. Malavasi, P. Postorino, S. Satpathy, V.V. Struzhkin, Origin of colossal magnetoresistance in LaMnO3 manganite, Proc. Natl. Acad. Sci. U. S. A. 112 (2015) 10869−10872, https://doi.org/10.1073/pnas.1424866112.
[6] V. Markovich, A. Wisniewski, H. Szymczak, Magnetic properties of perovskite manganites and their modifications, in: Handb. Magn. Mater, 2014, pp. 1−201, https://doi.org/10.1016/B978-0-444-63291-3.00001-5.
[7] T. Kimura, G. Lawes, T. Goto, Y. Tokura, A.P. Ramirez, Magnetoelectric phase diagrams of orthorhombic RMnO3 (R=Gd, Tb, and Dy), Phys. Rev. B Condens. Matter 71 (2005), https://doi.org/10.1103/PhysRevB.71.224425.
[8] J.B. Goodenough, Theory of the role of covalence in the perovskite-type manganites [La,M(II)]MnO3, Phys. Rev. 100 (1955) 564−573, https://doi.org/10.1103/PhysRev.100.564.
[9] P.G. De Gennes, Effects of double exchange in magnetic crystals, Phys. Rev. 118 (1960) 141−154, https://doi.org/10.1103/PhysRev.118.141.
[10] Y. Tokura, S. Seki, N. Nagaosa, Multiferroics of spin origin, Rep. Prog. Phys. 77 (2014), https://doi.org/10.1088/0034-4885/77/7/076501.
[11] M.H. Phan, S.C. Yu, Review of the magnetocaloric effect in manganite materials, J. Magn. Magn Mater. 308 (2007) 325−340, https://doi.org/10.1016/j.jmmm.2006.07.025.
[12] A. Muñoz, J.A. Alonso, M.J. Martìnez-Lope, J.L. García-Muñoz, M.T. Fernández-Díaz, Magnetic structure evolution of NdMnO3 derived from neutron diffraction data, J. Phys. Condens. Matter 12 (2000) 1361−1376, https://doi.org/10.1088/0953-8984/12/7/319.
[13] D.K. Pandey, A. Modi, N.K. Gaur, Revealing the structural and magnetic susceptibility aspects of Sr2+ substituted Y2-xSrxNiMnO6 ($0 \leq x \leq 0.1$) compounds, J. Appl. Phys. 126 (2019), https://doi.org/10.1063/1.5113843.
[14] G. Leinweber, D.P. Barry, M.J. Trbovich, J.A. Burke, N.J. Drindak, H.D. Knox, R.V. Ballad, R.C. Block, Y. Danon, L.I. Severnyak, Neutron capture and total cross-section measurements and resonance parameters of gadolinium, Nucl. Sci. Eng. 154 (2006) 261−279, https://doi.org/10.13182/NSE05-64.
[15] E. Dagotto, T. Hotta, A. Moreo, Colossal magnetoresistant materials: the key role of phase separation, Phys. Rep. 344 (2001) 1−153, https://doi.org/10.1016/S0370-1573(00)00121-6.
[16] R. Kajimoto, H. Yoshizawa, Y. Tomioka, Y. Tokura, Stripe-type charge ordering in the metallic A-type antiferromagnet (formula presented), Phys. Rev. B Condens. Matter 66 (2002) 1−4, https://doi.org/10.1103/PhysRevB.66.180402.
[17] Y. Tokura, Critical features of colossal magnetoresistive manganites, Rep. Prog. Phys. 69 (2006) 797−851, https://doi.org/10.1088/0034-4885/69/3/R06.
[18] Y. Tomioka, Y. Tokura, Global phase diagram of perovskite manganites in the plane of quenched disorder versus one-electron bandwidth, Phys. Rev. B Condens. Matter 70 (2004), https://doi.org/10.1103/PhysRevB.70.014432.
[19] M. Kenzelmann, A.B. Harris, S. Jonas, C. Broholm, J. Schefer, S.B. Kim, C.L. Zhang, S.W. Cheong, O.P. Vajk, J.W. Lynn, Magnetic inversion symmetry breaking and ferroelectricity in TbMnO3, Phys. Rev. Lett. 95 (2005), https://doi.org/10.1103/PhysRevLett.95.087206.
[20] H. Agarwal, P. Yadav, N.P. Lalla, J.A. Alonso, O.N. Srivastava, M.A. Shaz, Structural correlation of magneto-electric coupling in polycrystalline TbMnO3 at low temperature, J. Alloys Compd. 806 (2019) 510−519, https://doi.org/10.1016/j.jallcom.2019.07.228.
[21] J.M. De Teresa, C. Ritter, P.A. Algarabel, S.M. Yusuf, J. Blasco, A. Kumar, C. Marquina, M.R. Ibarra, Detailed neutron study of the crossover from long-range to short-range magnetic ordering in (Nd1-x Tbx) 0.55 Sr0.45 Mn O3 manganites, Phys. Rev. B Condens. Matter 74 (2006), https://doi.org/10.1103/PhysRevB.74.224442.
[22] M. Staruch, M. Jain, Long-range magnetic ordering in bulk Tb1-xMxMnO 3 (M = Ca, Sr), J. Phys. Condens. Matter 25 (2013), https://doi.org/10.1088/0953-8984/25/29/296005.
[23] H. Nhalil, S. Elizabeth, Estimation of Joule heating and its role in nonlinear electrical response of Tb0.5Sr0.5MnO3 single crystal, Solid State Commun. 248 (2016) 6−10, https://doi.org/10.1016/j.ssc.2016.09.005.
[24] Y. Jin, X.P. Cui, J.A. Cheng, S.X. Cao, W. Ren, J.C. Zhang, Spin reversal and ferroelectricity in perovskite Dy0.7Sr0.3MnO3 and Dy0.6Sr0.4MnO3, Appl. Phys. Lett. 107 (2015), https://doi.org/10.1063/1.4929155.
[25] K. Yadagiri, R. Nithya, A.T. Satya, K. Sethupathi, Evidence for ferromagnetic clusters at room temperature in Dy and Mn site co-substituted compounds: Dy0.55Sr0.45Mn1-xFexO3, J. Alloys Compd. 792 (2019) 411−417, https://doi.org/10.1016/j.jallcom.2019.04.018.
[26] V. Petrícek, M. Dušek, L. Palatinus, Crystallographic computing system JANA2006: general features, Zeitschrift Fur Krist 229 (2014) 345−352, https://doi.org/10.1515/zkri-2014-1737.
[27] G.E. Bacon, K. Lonsdale, Neutron diffraction, reports, Prog. Phys. 16 (1953) 1−61, https://doi.org/10.1088/0034-4885/16/1/301.
[28] P. Fischer, G. Frey, M. Koch, M. Konnecke, V. Pomjakushin, J. Schefer, R. Thut, N. Schlumpf, R. Burge, U. Greuter, S. Bondt, E. Berruyer, High-resolution powder diffractometer HRPT for thermal neutrons at SINQ, Phys. B Condens. Matter 276−278 (2000) 146−147, https://doi.org/10.1016/S0921-4526(99)01399-X.
[29] J. Rodríguez-Carvajal, Recent advances in magnetic structure determination by neutron powder diffraction, Phys. B Phys. Condens. Matter. 192 (1993) 55−69, https://doi.org/10.1016/0921-4526(93)90108-I.
[30] J. Rodríguez-Carvajal, Introduction to the Program FULLPROF: Refinement of Crystal and Magnetic Structures from Powder and Single Crystal Data, vol. 91191, Lab. Léon Brillouin (CEA-CNRS), CEA/Saclay, Gif Sur Yvette Cedex,-FRANCE, 2015.
[31] J. Rodr, A Program for Calculating Irreducible Representation of Little Groups and Basis Functions of Polar and Axial Vector Properties, Juan Rodríguez-Carvajal (LLB 2004), Solid State Phenom, 2004.
[32] J.A. Mydosh, Spin glasses: redux: an updated experimental/materials survey, Reports Prog, Phys 78 (2015), https://doi.org/10.1088/0034-4885/78/5/052501.

[33] O. Peña, M. Bahout, K. Ghanimi, P. Duran, D. Gutierrez, C. Moure, Spin reversal and ferrimagnetism in (Gd, Ca)MnO3, J. Mater. Chem. 12 (2002) 2480–2485, https://doi.org/10.1039/b202079n.
[34] B.C. Zhao, Y.Q. Ma, W.H. Song, Y.P. Sun, Magnetization steps in the phase separated manganite La0.275Pr0.35Ca0.375MnO3, Phys. Lett. Sect. A Gen. At. Solid State Phys. 354 (2006) 472–476, https://doi.org/10.1016/j.physleta.2006.01.088.
[35] E. Bousquet, A. Cano, Non-collinear magnetism in multiferroic perovskites, J. Phys. Condens. Matter 28 (2016), https://doi.org/10.1088/0953-8984/28/12/123001.